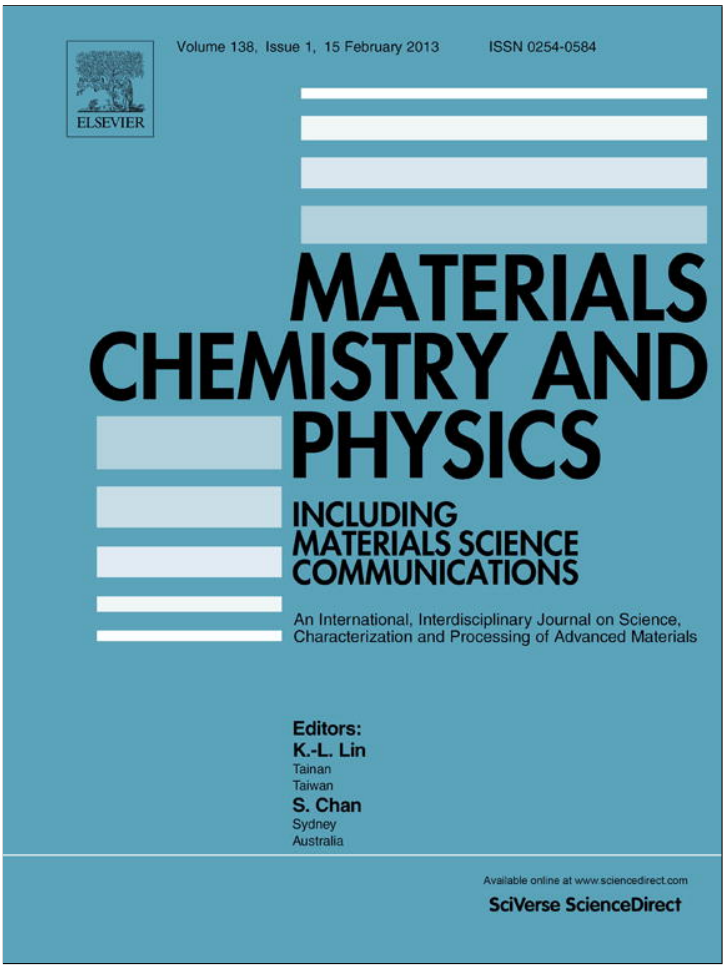

Materials Chemistry and Physics 138 (2013) 124–130

Contents lists available at SciVerse ScienceDirect

Materials Chemistry and Physics

journal homepage: www.elsevier.com/locate/matchemphys

Ultralow-temperature hydrothermal synthesis of Zn–Mn spinel nanocrystals: Its defect spinel of λ-MnO_2 prepared by a soft chemical method

Lili Xue, Zhong-Shuai Wu, Chunhua Ge, Xiang-Dong Zhang*

College of Chemistry, Liaoning University, Shenyang 110036, PR China

HIGHLIGHTS

- Ultralow-temperature hydrothermal synthesis of Zn–Mn spinel nanocrystals.
- Synthetic parameters were systematically investigated.
- Tetragonal-phase Zn–Mn spinel.
- Synthesis of λ-MnO_2 from $ZnMn_2O_4$ nanocrystals by a soft chemical method.

GRAPHICAL ABSTRACT

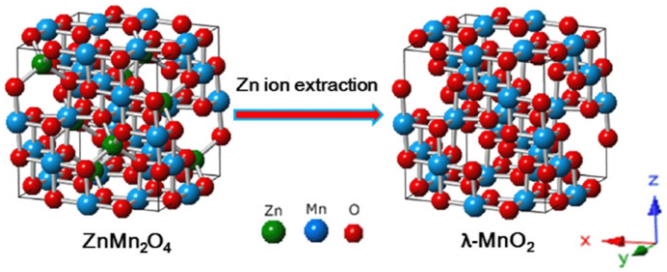

ARTICLE INFO

Article history:
Received 5 April 2012
Received in revised form
29 October 2012
Accepted 7 November 2012

Keywords:
Hydrothermal
Spinel
Zinc manganese oxide
MnO_2
Redox
Soft chemical method

ABSTRACT

An ultralow-temperature hydrothermal strategy was for the first time reported to synthesize spinel-type zinc manganese oxide ($ZnMn_2O_4$) nanocrystals at 70 °C. The synthetic parameters including hydrothermal temperature, zinc or manganese source, hydrothermal time, and NaOH concentration were systematically investigated. The structure and morphology characterization revealed that the resulting Zn–Mn spinels are tetragonal-phase, and have well-defined crystalline structure with the size of 10–20 nm. Furthermore, a defect spinel of λ-MnO_2 nanocrystal (10–20 nm) was directly synthesized from $ZnMn_2O_4$ nanocrystal upon acid leaching. Finally, a redox mechanism for the formation of λ-MnO_2 was discussed.

1. Introduction

Spinel-type transition metal oxides have attracted intensive research interests due to their fantastic magnetic, electronic, and thermal properties and various functional applications, which are closely associated with the distribution and valence state of metal ions caused by the Jahn–Teller effect in spinels [1–8]. Among them, the AB_2O_4-type spinels are the most important spinels [1–4,9], in which the tetrahedral (A) sites stand for d_4, d_9 metal ions and octahedral (B) sites represent for d_3, d_4, d_8, d_9 metal ions that are coordinated by the close-packed arrangement of oxygen ions.

Zinc manganese oxide ($ZnMn_2O_4$) is a normal AB_2O_4-type spinel with a tetragonal structure (Scheme 1) [10,11]. The Zn^{2+} cations with the d_{10} electronic configuration have a strong preference for occupying A sites and can highly stabilize the spinel structure. In contrast, the Mn^{3+} (d_4) ions located on the B sites exhibit a strong Jahn–Teller effect to produce the tetragonally deformed spinel, resulting in various fantastic properties and applications [12–21]. For instance, Zn–Mn spinels are widely used as negative temperature coefficient thermistors [12], diluted magnetic semiconductor materials [13], Zn–Mn batteries [14–16],

* Corresponding author. Tel.: +86 24 82031202; fax: +86 24 62202380.
E-mail address: xd623@sina.com (X.-D. Zhang).

0254-0584/$ – see front matter © 2012 Elsevier B.V. All rights reserved.
http://dx.doi.org/10.1016/j.matchemphys.2012.11.029

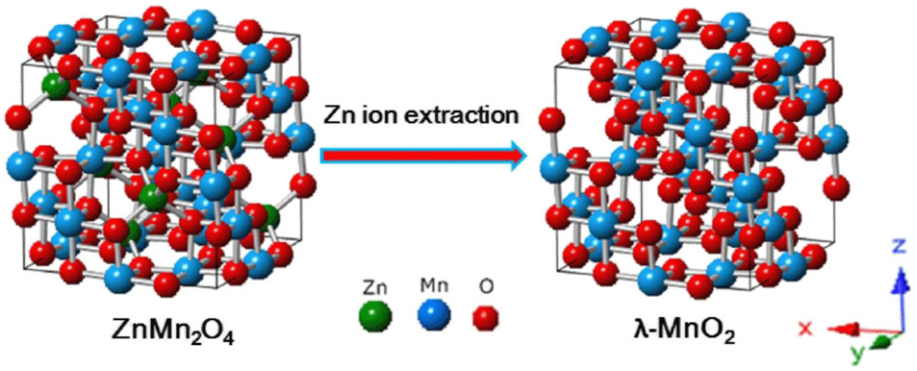

Scheme 1. Representation of the unit cell of $ZnMn_2O_4$ spinel prepared by ultralow-temperature hydrothermal synthesis and λ-MnO_2 defect spinel obtained from $ZnMn_2O_4$ by acid leaching.

catalyst [17], photocatalytic hydrogen production [18], and precursors of porous materials [19,20]. So far, the solid-state reaction is the most conventional method that can be used to directly synthesize Zn–Mn spinels from the precursors of zinc oxide and manganese oxide [3,4,22]. Unfortunately, this method requires high temperature (>1000 °C), long reaction time, and suffers from broad distribution in particle size and irregular in morphology [22]. To overcome this obstacle, several methods have been developed. For instance, Blasco et al. reported the facile synthesis of $ZnMn_2O_4$ by using soft synthetic conditions and highly reactive precursors of ZnO and $MnCO_3$ selectively heated at 400–800 °C in air. However, This approach involved in several steps including gel formation, calcinations, pressing into pellets and heating at high temperature [10]. Li et al. developed a lower temperature (500–800 °C) method that can significantly shorten reaction time to synthesize high crystalline $ZnMn_2O_4$ from $Zn(CH_3COO)_2{\cdot}2H_2O$ and $MnCl_2{\cdot}6H_2O$, but it still suffers from the generation of impurity phase and big size of irregular particles (600–700 nm) [23]. Recently, Menaka et al. reported a precursor mediated low-temperature (250 °C) route to fabricate the defect spinels of zinc manganese oxide nanospheres and nanorods. After heating, a refluxed process involved in acetic acid was used to remove the excess zinc oxide [21]. Although great efforts have been made, the large-scale, low-cost and low-temperature strategies to synthesize nanostructured $ZnMn_2O_4$ spinel still remains a great challenge.

Hydrothermal synthesis is a relatively mild, economical and versatile method to prepare low-dimensional nanomaterials with controllable size and shape [24,25]. Our group firstly reported the hydrothermal synthesis of the nanocrystalline $ZnMn_2O_4$ spinel, which was directly prepared from the phase transformation of birnessite-type layered manganese oxide treated at 170 °C for 48 h [26]. The as-prepared spinel has a homogenous size of 20–50 nm and high-quality crystalline structure [26]. In this work, we firstly developed an ultralow-temperature hydrothermal strategy to synthesize Zn–Mn spinel nanocyrstals with size of 10–20 nm, starting from $Zn(CH_3COO)_2{\cdot}2H_2O$ and $Mn(CH_3COO)_2{\cdot}2H_2O$ oxidized by H_2O_2 in the presence of NaOH for 2–48 h at 70 °C. The synthetic parameters including hydrothermal temperature, zinc or manganese source, hydrothermal time and NaOH concentration were systematically investigated. It was found that these parameters play important roles in the controllable formation of Zn–Mn spinel nanocrystals. Importantly, the Zn^{2+} ions can be well extracted from the resulting Zn–Mn spinel under acid conditions to prepare spinel-type manganese dioxide (λ-MnO_2, Scheme 1). Finally, a redox mechanism for Zn^{2+} extraction was proposed to elucidate the phase conversion of $ZnMn_2O_4$ to λ-MnO_2.

2. Experimental

2.1. Synthesis of Zn–Mn spinel

Typically, a mixed solution of 0.91 mL H_2O_2 (3%) and 8 mL NaOH (0.6 M) was slowly added into a Teflon lined stainless steel autoclave containing 0.8 mmol zinc salt ($Zn(CH_3COO)_2{\cdot}2H_2O$) and 1.6 mmol manganese salt ($Mn(CH_3COO)_2{\cdot}2H_2O$) while vigorously stirring. After that, the solution was maintained for 15 min at room temperature. Then, the precipitate was hydrothermally treated at 50–170 °C for 2–168 h under hydrothermal conditions. Finally, the samples were filtered, washed with distilled water three times, and dried overnight at 70 °C.

2.2. Synthesis of λ-MnO_2 by acid leaching

The Zn–Mn spinel (20 mg) was treated in the 100 mL aqueous solution of HNO_3 (0.5–13 M) for 3–7 days under continuous stirring condition. The solution after acid leaching was changed by the fresh acid solution every day. Finally, the sample was filtrated, washed with distilled water and dried overnight at 70 °C.

2.3. Materials characterization

Powder X-ray diffraction (XRD) analysis was performed on D-MAX/2400 with a Rigaku Multiflex powder diffractometer with Cu Ka radiation (λ = 1.540600 Å) between 10° and 60°. The chemical composition was determined using inductively coupled plasma (ICP-AES, Nippon Jarrel Ash, ICAP575II) after the sample was dissolved in the solution of HNO_3 and H_2O_2. Thermogravimetric analysis/differential thermal analysis (TG-DTA) was performed at a heating rate of 10 °C min^{-1} in air with an METTLER TGA/SDTA851e thermogravimetric analyzer. The morphologies of the samples were characterized by transmission electron microscopy (TEM, JEX-100SX) and high resolution transmission electron microscopy (HRTEM, Philips Tecnai F20). X-ray photoelectron spectra (XPS) were collected on a ThermoESCALAB 250 X-ray photoelectron spectrometer, using nonmonochromatized Al Ka X-ray as the excitation source.

3. Results and discussion

3.1. The effect of hydrothermal temperature

Fig. 1 shows the XRD patterns of the samples synthesized hydrothermally for 24 h at different temperature. As seen in Fig. 1, Zn–Mn spinel ($ZnMn_2O_4$, JCPDS24-1133) with the tetragonal

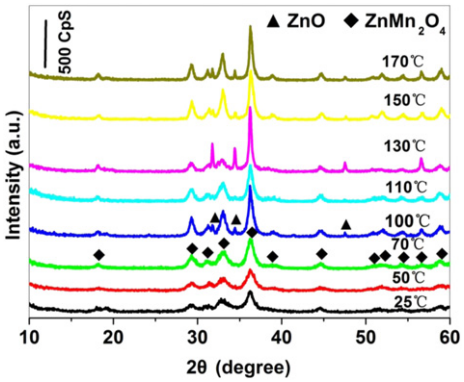

Fig. 1. XRD patterns of the samples hydrothermally synthesized at different temperature of 25–170 °C.

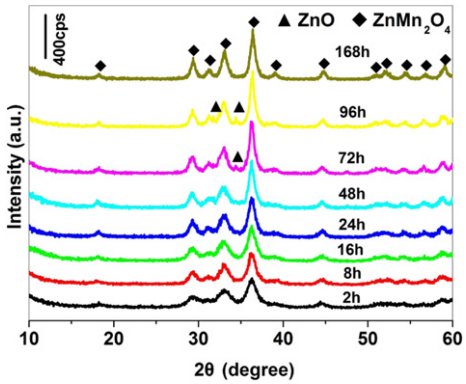

Fig. 3. XRD patterns of the samples hydrothermally synthesized at 70 °C for different time.

structure was formed from $Zn(CH_3COO)_2{\cdot}2H_2O$ by oxidation of H_2O_2 in the alkaline condition (NaOH) at room temperature, and the intensities of all the diffraction peaks were gradually increased with increasing hydrothermal temperature until 70 °C. Beyond this temperature, the diffraction peaks of zinc oxide (ZnO, JCPDS36-1451) appeared at 31.76, 34.44, 47.52 were observed. It was assumed that the H_2O_2 decomposition at higher temperature (100 °C – 170 °C) destroy the original reaction ratios of the used reactants (Zn^{2+}, Mn^{2+} and H_2O_2), thus resulting in the formation of ZnO phase.

3.2. The effect of the anions

After optimizing hydrothermal temperature, the effect of the anions of zinc/manganese sources on the formation of Zn–Mn spinel was further investigated. The parallel zinc/manganese salts with the same anions were $ZnCl_2/MnCl_2$, $Zn(NO_3)_2/Mn(NO_3)_2$, $ZnSO_4/MnSO_4$, $Zn(CH_3COO)_2/Mn(CH_3COO)_2$, respectively. As seen in Fig. 2, the XRD results suggested that the single-phase Zn–Mn spinels (JCPDS24-1133) were obtained at different anion conditions. Differently, the diffraction intensities gradually increase from Cl^-, NO_3^-, SO_4^{2-}, to $C_2H_3O_2^-$ anions, indicative of the favorable formation of Zn–Mn spinel in the condition of $C_2H_3O_2^-$ anions. Therefore, it was concluded that the effect of anions on the formation of Zn–Mn spinels can be described as follows: $C_2H_3O_2^- > SO_4^{2-} > NO^{3-} > Cl^-$. The superiority of $C_2H_3O_2^-$ anions over the other anions was attributed to the hydrophobic effect of $C_2H_3O_2^-$ anions served as a surfactant with carbon hydrogen chain [27].

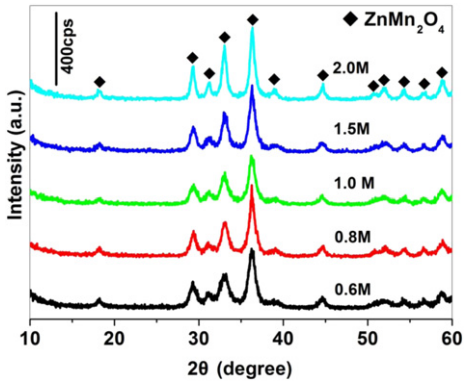

Fig. 4. XRD patterns of the samples synthesized hydrothermally at 70 °C for 24 h in different NaOH concentration.

3.3. The effect of hydrothermal time

Hydrothermal time also is an important parameter in the formation of Zn–Mn spinel [26]. Fig. 3 shows the XRD patterns of the samples hydrothermally synthesized at 70 °C between 2 h and 168 h. It was observed that Zn–Mn spinel (JCPDS24-1133) was formed after 2 h, and the intensities of the diffraction peaks of Zn–Mn spinel increase with increasing hydrothermal time up to 48 h, and no impurity phase of ZnO was observed. When hydrothermal time is extended, for example, for 72 h and 96 h, the ZnO phase was

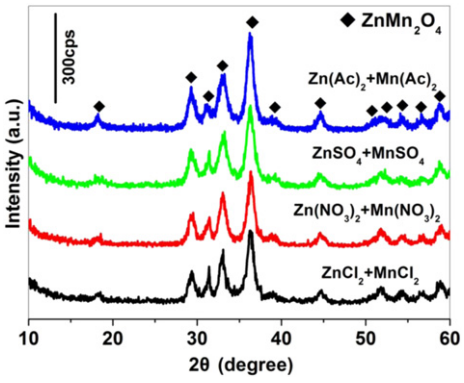

Fig. 2. XRD patterns of the samples hydrothermally synthesized at 70 °C for 24 h in different zinc/manganese sources containing the same anions.

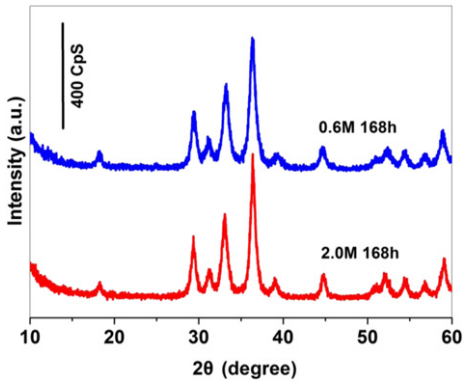

Fig. 5. XRD patterns of the Zn–Mn spinels synthesized hydrothermally at 70 °C for 168 h at the NaOH concentration of 0.6 M (up) and 2.0 M (down), respectively.

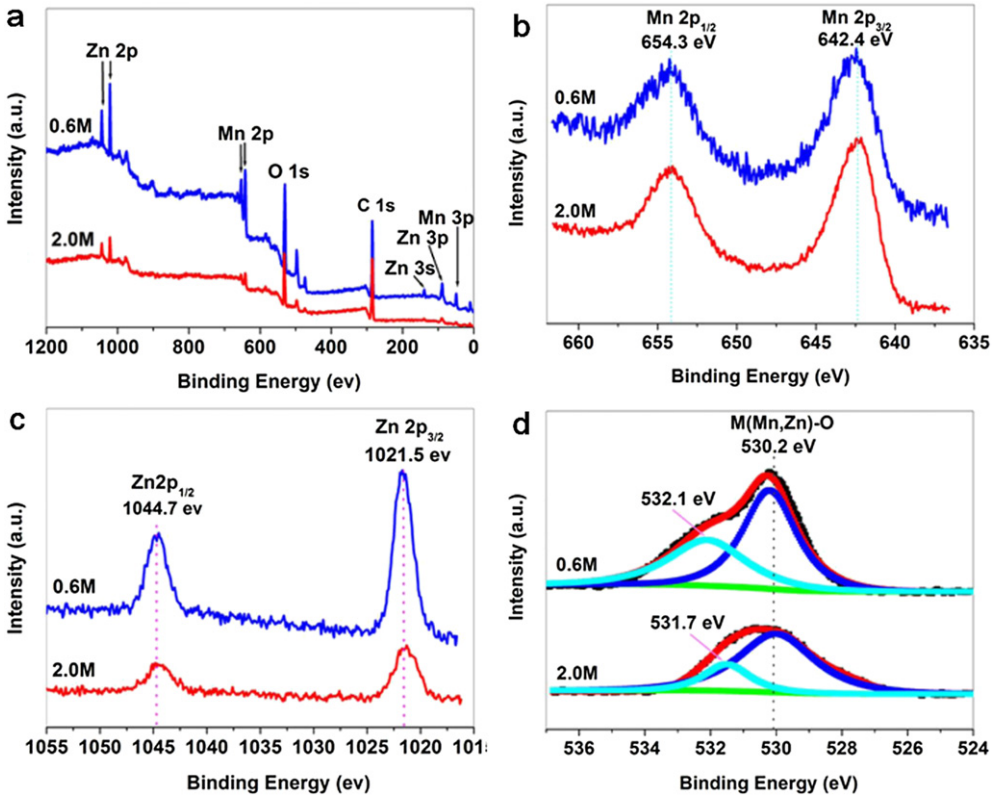

Fig. 6. (a) XPS, (b) Mn 2P, (c) Zn 2p and (d) O 1s spectra of the Zn–Mn spinels synthesized hydrothermally at 70 °C for 168 h at 0.6 M (up) and 2.0 M (down) NaOH, respectively.

partly precipitated together with Zn–Mn spinel. More than 96 h, the single-phase Zn–Mn spinel was hydrothermally obtained again. Additionally, it was noted that the diffraction peaks of Zn–Mn spinel appeared in the XRD patterns were gradually weaker and broader, which indicated that the size of nanocrystals could make for the smaller nanoparticles.

3.4. The effect of NaOH concentration

Fig. 4 shows the XRD patterns of the samples synthesized hydrothermally at 70 °C for 24 h in different NaOH concentration of 0.6, 0.8, 1.0, 1.5 and 2.0 M, respectively. When NaOH concentration is 0.6 M, the pH value of reaction solution after hydrothermal reaction is 7, suggesting that NaOH was fully taken part in the reaction during $ZnMn_2O_4$ formation. When the NaOH concentration used is higher than 0.6 M, the intensities of the diffraction peaks increase. This result suggests that the higher the NaOH concentration used, the better the crystallinity of Zn–Mn spinels.

To gain the more insight of the effect of NaOH concentration on the distribution and valence state of zinc and manganese ions, we chose the optimized hydrothermal condition to synthesize the Zn–Mn spinels from $Zn(CH_3COO)_2{\cdot}2H_2O$ and $Mn(CH_3COO)_2{\cdot}2H_2O$ oxidized by H_2O_2 at 70 °C for 168 h, and the NaOH concentration used was 0.6 and 2.0 M, respectively. Fig. 5 shows the XRD patterns of these two as-prepared Zn–Mn spinel samples. Compared to the XRD patterns in Fig. 4, the intensities of the diffraction peaks in these two samples further increase because of increased hydrothermal time.

Fig. 6 shows the XPS of the Zn–Mn spinels synthesized hydrothermally at 70 °C for 168 h in the NaOH concentration of 0.6 and 2.0 M, respectively. It is clearly observed that the three elements of Zn, Mn and O are identified in the samples, as shown in Fig. 6a. As to the Mn 2p XPS spectra, two characteristic peaks at 654.3 and 642.4 eV are corresponding to the Mn $2p_{1/2}$ and Mn $2p_{3/2}$, respectively, demonstrating the presence of Mn^{3+} in the samples (Fig. 6b) [28,29]. Due to multiple splitting effects, the slight upshift (2.0 M NaOH) or downshift (0.6 M NaOH) tendency of binding energy in samples are closely related to the coexistence of trace Mn^{4+} or Mn^{2+} with Mn^{3+} in the samples [21,30]. The Zn 2p XPS spectrum is shown in Fig. 6c. The peaks at binding energy of 1044.7 and 1021.5 eV are attributed to the Zn $2p_{1/2}$ and Zn $2p_{3/2}$, respectively. And the O 1s spectrum can be deconvoluted into two peaks, as shown in Fig. 6d. One stronger peak with the binding energy of 530.2 eV is corresponding to the characteristics of oxygen in metal (Mn, Zn) oxide. The small shoulder peak around 531.7–532.1 eV is introduced by the adsorbed oxygen species, such as OH, H_2O, and carbonate groups on the surface [28]. Additionally, the XPS quantitative analysis reveals that the Zn:Mn ratio in the samples is

Table 1
Preparation conditions and element components of Zn–Mn spinels obtained hydrothermally at 70 °C for 168 h.

C_{NaOH} (M)	a (Å)[a]	c (Å)[a]	c/a	Z_{Mn}[b]	Zn/Mn	Composition	Cationic distribution [5,6]
0.6	5.720	9.246	1.6164	2.966	0.463	$Zn_{0.95}Mn_{2.05}O_{3.99}$	$Zn^{2+}_{0.95}Mn^{2+}_{0.05}[Mn^{3+}_{2.00}]O_4$
2.0	5.722	9.247	1.6158	3.058	0.571	$Zn_{1.09}Mn_{1.91}O_{4.01}$	$Zn^{2+}_{1.00}[Zn^{2+}_{0.09}Mn^{4+}_{0.09}Mn^{3+}_{1.82}]O_4$

[a] Lattice constant.
[b] Average valence of Mn.

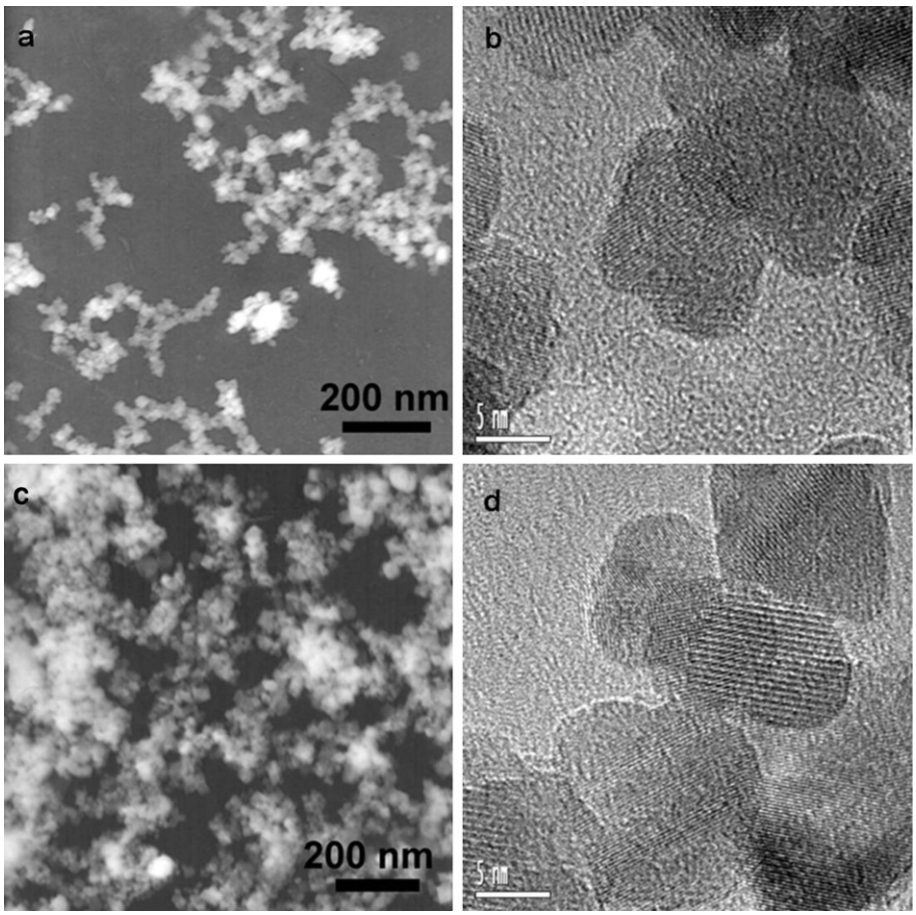

Fig. 7. TEM and HRTEM images of the samples synthesized hydrothermally at 70 °C for 168 h in the NaOH concentration of (a, b) 0.6 M and (c, d) 2.0 M.

basically equal to 1:2, identical to the formula of $ZnMn_2O_4$. These results can be further evidenced by ICP-AES analysis. Based on the results of both XPS and ICP-AES, the preparation condition, distribution and valence state of zinc and manganese ions of these two Zn–Mn spinel samples obtained hydrothermally at 0.6 and 2.0 M NaOH were summarized in Table 1. The formula obtained is $Zn^{2+}_{0.95}Mn^{2+}_{0.05}[Mn^{3+}_{2.00}]O_4$ in 0.6 M while that is $Zn^{2+}_{1.00}[Zn^{2+}_{0.09}Mn^{4+}_{0.09}Mn^{3+}_{1.82}]O_4$ in 2.0 M NaOH.

Fig. 7 shows the TEM images of the Zn–Mn spinels obtained hydrothermally at 70 °C for 168 h in the lower (0.6 M) and higher (2.0 M) NaOH concentration. It is observed that the average size of nanoparticles are about 10–20 nm with a uniform distribution in the lower NaOH concentration (Fig. 7a and b). In the higher alkaline condition (2.0 M), the nanocrystals tend to form aggregated particles (Fig. 7c and d). Importantly, both of them exhibit the nature of crystalline structure with well-defined textures (Fig. 7b and d). Therefore, it was confirmed that the NaOH concentration plays a key role in tuning the morphology, composition, distribution and valence state of zinc and manganese ions in Zn–Mn spinels. The lower NaOH concentration should be benefit for the crystalline process of Zn–Mn nanocrystals with a narrow-size distribution and less agglomeration.

3.5. Thermal analysis of Zn–Mn spinel

To investigate the thermal stability, the TG/DTA analysis was carried out from 25 to 800 °C in air. Fig. 8 shows the TG/DTA curves of Zn–Mn spinels obtained at 70 °C for 168 h when the NaOH concentration is (a) 0.6 M and (b) 2.0 M, respectively. As seen in Fig.8, there are two weight losses occurring in the regions of 50–150 °C and 200–700 °C in lower NaOH concentration, and of 200–400 °C and 500–700 °C in higher NaOH concentration, while their corresponding DTA curves exhibit one endothermic peak and one exothermic peak. In the case of 0.6 M NaOH, the first weight loss of the sample in Fig. 8a below 150 °C can be ascribed to the evaporation of the absorbed water [26]. The second slow weight loss in the regions of 200–700 °C corresponds to the loss of the oxygen excess δ in $Zn_xMn_{3-x}O_{4+\delta}$ and partly phase transformation from $ZnMn_2O_4$ to $ZnMnO_3$ [7,31]. In the case of 2.0 M, the weight loss starting from 200 °C is attributed to the nonstoichiometric oxygen (δ) and the phase transformation from tetragonal $ZnMn_2O_4$

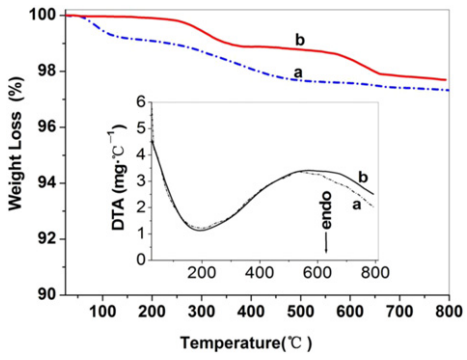

Fig. 8. TG and DTA curves (Inset) of the samples synthesized hydrothermally at 70 °C for 7 days in the NaOH concentration of (a) 0.6 M and (b) 2.0 M.

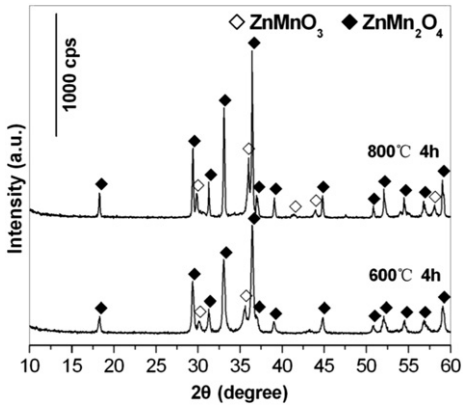

Fig. 9. XRD patterns of the samples obtained from $ZnMn_2O_4$ heated at the temperature of 600 °C and 800 °C for 4 h in air.

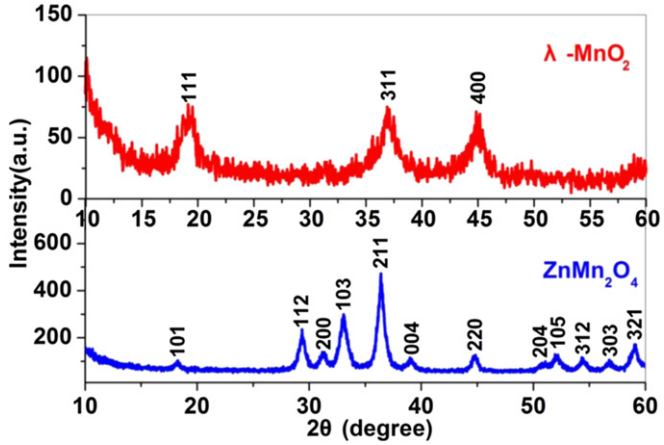

Fig. 10. (a) XRD patterns of as-prepared $ZnMn_2O_4$ (down) and λ-MnO_2 (up) treated by 1.0 M HNO_3 leaching for 3 days.

into cubic $ZnMnO_3$. To demonstrate the presence of $ZnMnO_3$ phase, we further performed the XRD patterns of the samples obtained from $ZnMn_2O_4$ calcined in 600 °C and 800 °C for 4 h in air, as shown in Fig. 9. This can give a clear evidence of $ZnMnO_3$ presented in the calcined samples before and after 600 °C, which leads to the oxygen loss. More importantly, the weight loss at the whole temperature range only reaches ~2.51% in Fig. 8a and ~2.31% in Fig. 8b, respectively, demonstrating that the tetragonal Zn–Mn spinels have high thermal stability [31].

3.6. Synthesis of λ-MnO_2 from $ZnMn_2O_4$

λ-MnO_2 is one metastable form of manganese dioxides with a three-dimensional network of tunnels connecting vacant sites in the oxide lattice. This defect spinel of λ-MnO_2 exhibits unusual magnetic properties due to its geometrically frustrated systems [32–35]. In 1981, Hunter firstly reported this new crystal form of manganese dioxide (λ-MnO_2) prepared by acid leaching of lithium from the spinel $LiMn_2O_4$, which can preserve the structural framework of the $LiMn_2O_4$ [32]. Until now, most of the works reported that the preparation of λ-MnO_2 was focused on the conversion of $LiMn_2O_4$ to λ-MnO_2 by acid or electrochemical leaching [32–35]. In this work, we firstly attempted to synthesize λ-MnO_2 from the $ZnMn_2O_4$ spinels by a soft chemical method (Scheme 1).

Fig. 10 shows the XRD patterns of λ-MnO_2 obtained from $ZnMn_2O_4$ treated by 1.0 M HNO_3 leaching for 3 days. The XRD patterns show that the three main peaks of the d111, d311, d400 are assigned to λ-MnO_2 (JCPDS44-0992), manganese dioxide spinel (Fig. 10) [33,34]. TEM and HRTEM images of the as-prepared λ-MnO_2 were shown in Fig. 11. It is observed that the average size of the nanoparticles with well crystalline nature are about 10–20 nm, which is in good agreement with that of $ZnMn_2O_4$ precursor. Fig. 12a shows the XRD of λ-MnO_2 obtained from Zn–Mn spinels treated for 7 days by the different HNO_3 concentration of 0.5, 0.1, 0.2 and 13 M, respectively. It was revealed that the increase of the acid concentration has no significant influence of the resulting λ-MnO_2. Fig. 12b shows the TG curves of λ-MnO_2 obtained from $ZnMn_2O_4$ treated by the different concentration of HNO_3 for 7 days. There are two main weight losses occurring in the regions of 50–200 °C and 200–600 °C. The weight loss of the samples below 200 °C can be ascribed to the evaporation of the absorbed water, and the second weight loss about ~10% in the regions of 200–600 °C corresponds to the oxidation of λ-MnO_2 to Mn_2O_3, which leads to the oxygen loss [32].

Several studies had discussed the extraction/insertion mechanism of Li^+ in the $LiMn_2O_4$ spinels. Generally, two metal extraction mechanisms were provided: ion-exchanged reaction and redox reaction [32–36]. Taking our present work into consideration, zinc manganese oxide $\{(Zn^{II})_T[Mn^{III}_2]_OO_4\}$ obtained is one of typical spinels with the 1 × 3 tunnel structure [36], and the divalent Zn^{II}

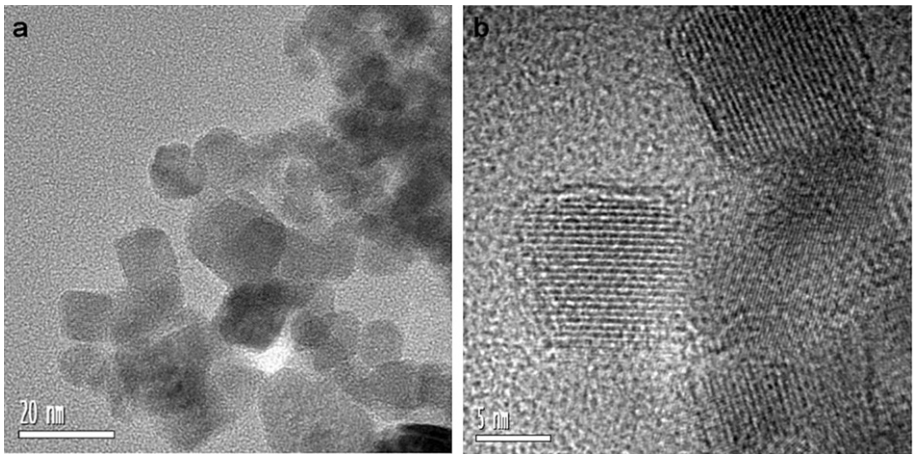

Fig. 11. (a) TEM and (b) HRTEM images of λ-MnO_2 treated by 1.0 M HNO_3 leaching for 3 days.

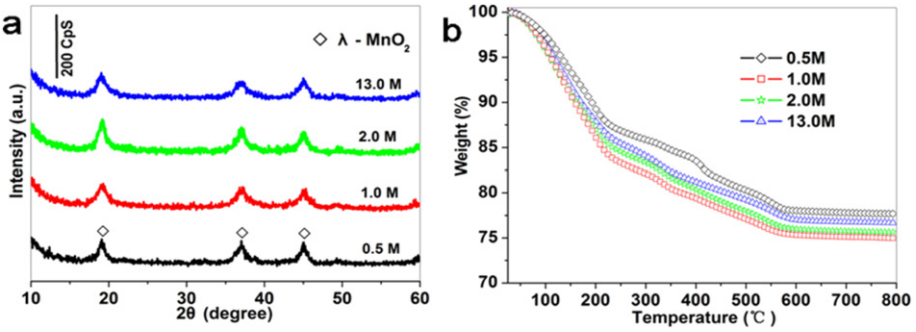

Fig. 12. (a) XRD patterns and (b) TG curves of λ-MnO_2 obtained from $ZnMn_2O_4$ treated by the different concentration of HNO_3 for 7 days.

ions are at the A tetrahedral sites and the trivalent Mn^{III} ions are at the B octahedral sites. We proposed a redox mechanism for Zn^{2+} ion removal from $ZnMn_2O_4$ spinel upon acid leaching:

$$2(Zn)\left[Mn_2^{III}\right]O_4 + 8H^+ = ()\left[Mn_2^{IV}\right]O_4 + 2Zn^{2+} + 2Mn^{2+} + 4H_2O$$

In this reaction, Mn^{III} ions are disproportionated to Mn^{IV} and Mn^{II} under acidic conditions, which can be described: $Mn^{III} \rightarrow 1/2Mn^{IV} + 1/2Mn^{II}$. All Mn atoms in the defect spinel of λ-MnO_2 are tetravalent after Zn^{2+} ion extraction. Because such spinel-type manganese oxide has empty tetrahedral sites, therefore, other metal ions under certain circumstance can enter the empty tetrahedral sites to obtain new functional magnetic and electrode materials for potential applications.

4. Conclusions

An ultralow-temperature hydrothermal strategy was developed to synthesize spinel-type $ZnMn_2O_4$ nanocrystals with the size of about 10–20 nm at 70 °C. It was found that the synthetic parameters, including hydrothermal temperature, zinc or manganese source, hydrothermal time, and NaOH concentration, play important roles in the controllable formation of Zn–Mn spinels. Furthermore, the Zn^{2+} ions were successfully extracted from the resulting Zn–Mn spinel under acidic condition and thus a defect spinel of manganese dioxide (λ-MnO_2) nanocrystal was prepared. Finally, a redox mechanism was proposed to elucidate the phase conversion of $ZnMn_2O_4$ to λ-MnO_2. It is believed that, compared to the other reported methods, hydrothermal method is a more promising low-cost and low-temperature method to fabricate nanostructured Zn–Mn spinels and its derivatives of λ-MnO_2, which may have great potential for applications in magnetic and electrode materials etc.

Acknowledgments

This work was financially supported by the National Natural Science Foundation of China under Grant Nos. 20971062/B010303 and 21171081/B0103.

References

[1] E.J.W. Verwey, E.L. Heilmann, J. Chem. Phys. 15 (1947) 174.
[2] E.J. Verwey, P.W. Haayman, F.C. Romeijn, J. Chem. Phys. 15 (1947) 181.
[3] J.D. Dunitz, L.E. Orgel, J. Phys. Chem. Solids 3 (1957) 20.
[4] J.D. Dunitz, L.E. Orgel, J. Phys. Chem. Solids 3 (1957) 318.
[5] Y.N. Venevtsev, D.F. Dzmuhadze, N.V. Fadeeva, S.A. Ivanov, Ferroelectrics 79 (1988) 523.
[6] H. Aoki, H. Kamimura, Solid State Commun. 63 (1987) 665.
[7] S. Fritsch, J. Sarrias, M. Brieu, J.J. Couderc, J.L. Baudour, E. Snoeck, A. Rousset, Solid State Ionics 109 (1998) 229.
[8] J.M. Paulsen, J.R. Dahn, Chem. Mater. 11 (1999) 3065.
[9] G. Pistoia, A. Antonini, R. Rosati, C. Bellitto, G.M. Ingo, Chem. Mater. 9 (1997) 1443.
[10] J. Blasco, J. Garcia, J. Solid State Chem. 179 (2006) 2199.
[11] M. Peiteado, S. Sturm, A.C. Caballero, D. Makovec, Acta Mater. 56 (2008) 4028.
[12] C. Chanel, S. Fritsch, C. Drouet, A. Rousset, M.L.M. Sarrion, L. Mestres, M. Morales, Mater. Res. Bull. 35 (2000) 431.
[13] S. Lee, E.B. Song, K.L. Wang, C.S. Yoon, I.T. Yoon, Y. Shon, T.W. Kang, J. Phys. Chem. C 115 (2011) 23564.
[14] Y.F. Deng, S.D. Tang, Q.M. Zhang, Z.C. Shi, L.T. Zhang, S.Z. Zhan, G.H. Chen, J. Mater. Chem. 21 (2011) 11987.
[15] J.M. Nan, D.M. Han, M. Cui, M.J. Yang, L.M. Pan, J. Hazard. Mater. 133 (2006) 257.
[16] H. Yang, H.Q. Yang, Y.L. Lu, N. Li, B.X. Li, J. Power Sources 62 (1996) 223.
[17] J. Ziolkowski, A.M. Maltha, H. Kist, E.J. Grootendorst, H.J.M. deGroot, V. Ponec, J. Catal. 160 (1996) 148.
[18] Y. Bessekhouad, M. Trari, Int. J. Hydrogen Energy 27 (2002) 357.
[19] E.S. Toberer, R. Seshadri, Adv. Mater. 17 (2005) 2244.
[20] E.S. Toberer, J.P. Lofvander, R. Seshadri, Chem. Mater. 18 (2006) 1047.
[21] Menaka, S.L. Samal, K.V. Ramanujachary, S.E. Lofland, Govind, A.K. Ganguli, J. Mater. Chem. 21 (2011) 8566.
[22] S. Guillemet-Fritsch, C. Chanel, J. Sarrias, S. Bayonne, A. Rousset, X. Alcobe, M.L.M. Sarrion, Solid State Ionics 128 (2000) 233.
[23] H. Li, B. Song, W.J. Wang, X.L. Chen, Mater. Chem. Phys. 130 (2011) 39.
[24] W.T. Yao, S.H. Yu, Int. J. Nanotechnol. 4 (2007) 129.
[25] A.B. Djurisic, Y.Y. Xi, Y.F. Hsu, W.K. Chan, Recent Pat. Nanotechnol. 1 (2007) 121.
[26] X.D. Zhang, Z.S. Wu, J. Zang, L. Da, Z.D. Zhang, J. Phys. Chem. Solids 68 (2007) 1583.
[27] J. Luo, S.L. Suib, J. Phys. Chem. B 101 (1997) 10403.
[28] P. Zhang, X.Y. Li, Q.D. Zhao, S.M. Liu, Nanoscale Res. Lett. 6 (2011).
[29] J.F. Fernandez, A.C. Caballero, M. Villegas, S.J. Khatib, M.A. Banares, J.L.G. Fierro, J.L. Costa-Kramer, E. Lopez-Ponce, M.S. Martin-Gonzalez, F. Briones, A. Quesada, M. Garcia, A. Hernando, J. Eur. Ceram. Soc. 26 (2006) 3017.
[30] H.J. Noh, S. Yeo, J.S. Kang, C.L. Zhang, S.W. Cheong, S.J. Oh, P.D. Johnson, Appl. Phys. Lett. 88 (2006) 081911.
[31] T. Ishikawa, K. Tobe, T. Timura, T. Katsufuji, Y. Tokura, Phys. Rev. B 62 (2000) 12354.
[32] J.C. Hunter, J. Solid State Chem. 39 (1981) 142.
[33] Q. Feng, Y. Miyai, H. Kanoh, K. Ooi, Langmuir 8 (1992) 1861.
[34] J.E. Greedan, N.P. Raju, A.S. Wills, C. Morin, S.M. Shaw, J.N. Reimers, Chem. Mater. 10 (1998) 3058.
[35] B. Ammundsen, D.J. Jones, J. Roziere, H. Berg, R. Tellgren, J.O. Thomas, Chem. Mater. 10 (1998) 1680.
[36] Q. Feng, H. Kanoh, K. Ooi, J. Mater. Chem. 9 (1999) 319.